

Vibrational Spectroscopy of Water with High Spatial Resolution

Jacob R. Jokisaari,* Jordan A. Hachtel,* Xuan Hu, Arijita Mukherjee, Canhui Wang, Andrea Konecna, Tracy C. Lovejoy, Niklas Dellby, Javier Aizpurua, Ondrej L. Krivanek, Juan-Carlos Idrobo, and Robert F. Klie

The ability to examine the vibrational spectra of liquids with nanometer spatial resolution will greatly expand the potential to study liquids and liquid interfaces. In fact, the fundamental properties of water, including complexities in its phase diagram, electrochemistry, and bonding due to nanoscale confinement are current research topics. For any liquid, direct investigation of ordered liquid structures, interfacial double layers, and adsorbed species at liquid–solid interfaces are of interest. Here, a novel way of characterizing the vibrational properties of liquid water with high spatial resolution using transmission electron microscopy is reported. By encapsulating water between two sheets of boron nitride, the ability to capture vibrational spectra to quantify the structure of the liquid, its interaction with the liquid-cell surfaces, and the ability to identify isotopes including H_2O and D_2O using electron energy-loss spectroscopy is demonstrated. The electron microscope used here, equipped with a high-energy-resolution monochromator, is able to record vibrational spectra of liquids and molecules and is sensitive to surface and bulk morphological properties both at the nano- and micrometer scales. These results represent an important milestone for liquid and isotope-labeled materials characterization with high spatial resolution, combining nanoscale imaging with vibrational spectroscopy.

Understanding the fundamental properties of water, including anomalies in its phase diagram,^[1] electrochemistry,^[2] and changes in bonding due to nanoscale confinement,^[3] is central

to many research areas. We demonstrate that by encapsulating H_2O between 2D hexagonal boron nitride (h-BN) layers, it is now possible to quantify the structure of the liquid and its interaction with the hosting solid-state surfaces, as well as identify isotopes using electron energy-loss spectroscopy (EELS). The electron microscope used here, equipped with a high-energy-resolution monochromator, is shown to record vibrational spectra of liquids and molecules with signals sensitive to surface and bulk morphological properties of the liquid both at the nano and micrometer scales.^[4] These results are an important milestone for liquid and isotope-labeled materials characterization, combining nanoscale imaging with vibrational spectroscopy in an electron microscope.

Vibrational EELS in a monochromated scanning transmission electron microscope (STEM) is a recently developed approach^[4–11] that allows the characterization of surface species including OH groups attached to nanoparticles,^[5] organic

compounds such as the nucleobase guanine,^[9] and low-pressure ionic liquids adsorbed onto TEM substrates.^[12] The achievable energy resolution of the latest generation of monochromators has so far been 10–30 meV, but it has recently improved to 5 meV. Vibrational EELS in the STEM can be carried out in an “aloof” scattering geometry that provides nanometer-scale spatial resolution and minimizes radiation damage, thus avoiding a major obstacle for examining liquids in an electron microscope.^[6–8,11] Tip-enhanced Raman spectroscopy (TERS)^[13] and infrared scanning near-field optical microscopy (SNOM)^[14] have previously been employed to study organic compounds at nanoscale resolution. These methods rely on the interaction between a sharp etched tip and the sample, with the resolution limited by the tip–sample contact. The overall resolution limit of these scanning-probe techniques can be between 10 and 25 nm,^[13,14] and must be performed with the tip immersed in a liquid, or in a liquid cell geometry. In a liquid cell, the spatial resolution will be limited by the surface of the encapsulating membrane. Vibrational EELS within a STEM employs a different methodology and can be regarded as highly complementary to these surface probe techniques. The spatial resolution

Dr. J. R. Jokisaari, X. Hu, Dr. A. Mukherjee, Dr. C. Wang,^[+] Prof. R. F. Klie
Department of Physics
University of Illinois at Chicago
Chicago, IL 60607, USA
E-mail: jacobj@uic.edu

Dr. J. A. Hachtel, Dr. J.-C. Idrobo
Center for Nanophase Materials Sciences
Oak Ridge National Laboratory
Oak Ridge, TN 37831, USA
E-mail: hachtelja@ornl.gov

A. Konecna, Prof. J. Aizpurua
Center for Material Physics (CSIC-UPV/EHU) and DIPC
Donostia – San Sebastián Gipuzkoa 20018, Spain

Dr. T. C. Lovejoy, Dr. N. Dellby, Dr. O. L. Krivanek
Nion Company
11511 NE 118th St., Kirkland, WA 98034, USA

^[+]Present address: University of Maryland/NIST, Institute for Research in Electronics and Applied Physics, College Park, MD 20740, USA

DOI: 10.1002/adma.201802702

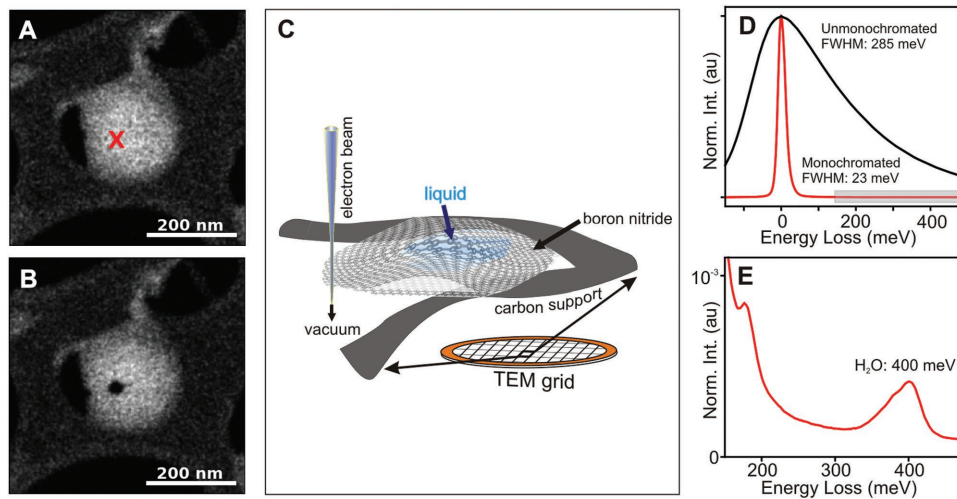


Figure 1. Aloof EELS of BN liquid cells. A,B) STEM images of a BN encapsulated water cell before and after e-beam irradiation. C) Illustration of aloof EELS measurements on a BNLC liquid cell. D) EEL spectra of the ZLP of unmonochromated (black) and monochromated (red) electron probes. E) The monochromated, aloof, vibrational response of an H_2O -filled BNLC with the O–H stretching phonon of water at 400 meV and a phonon peak at ≈ 180 meV, in the expected location of the h-BN phonon.^[25,27]

of EELS is limited by the delocalization of the low-angle scattered vibrational EELS signal and the potential for electron beam damage to the specimen. Resolutions of better than 1 nm have been reported in BN when the high angle scattered part of the vibrational signal is considered.^[15] The spectral resolution of vibrational EELS is lower than that of TERS or SNOM, but EELS is less sensitive toward surface states.

Vibrational EELS, then, is capable of probing a volume as well as surfaces, and does not require the interface to be fixed to the support substrate, allowing investigation of the properties of liquids and liquid interfaces themselves. In this work, we use vibrational EELS in the aloof mode to obtain vibrational data from liquid water confined in boron nitride liquid cells (BNLCs), shown schematically in Figure 1C. We demonstrate isotopic sensitivity of our approach by detection of the vibration energy of D_2O in a mixed $\text{H}_2\text{O}/\text{D}_2\text{O}$ sample. This work provides the first example of vibrational spectroscopy of liquid water and isotope identification in a transmission electron microscope. The combination of these developments creates a unique opportunity for nanoscale vibrational spectroscopy of water and other vacuum or atmosphere incompatible liquids. One major drawback for TEM characterization of liquids is the requirement for high vacuum. Recently, major effort has gone into the development of membrane-based electron microscopy liquid cell stages that encapsulate a small volume of liquid between thin silicon nitride membranes. When mounted on a chip, *in situ* (operando) liquid, electrochemical, and even vapor-phase measurements are now possible.^[16–18] Yet, the thickness of the window material and of the liquid droplet (usually >100 nm) limits the spatial resolution and generally precludes even core-loss EELS.^[19]

An alternate approach to encapsulating liquids employs graphene membranes to confine the liquid, allowing the creation of vacuum-stable nanosized liquid droplets.^[20–24] Although this yields much greater spatial resolution, it creates a problem for vibrational spectroscopy as graphene is a conductor. With a continuum of allowed energy transitions, and several phonon

modes of its own, the graphene window layers can cause a strong background signal in the low-loss region obscuring the liquid's vibrational peaks. To avoid this problem, we developed BNLC with liquid encapsulated in two layers of hexagonal boron nitride, a higher-bandgap 2D material, with essentially no EELS background up to 6 eV apart from the h-BN vibrational peaks at energies below 200 meV.^[25] The difference in background signal and radiolysis-induced bubble formation using h-BN over graphene in the liquid cells is discussed further in Figures S1 and S2 (Supporting Information).

Another potential obstacle to studying water in the electron microscope is its susceptibility to electron beam induced radiolysis even at fluxes as low as 0.5 electrons $\text{\AA}^{-2} \text{s}^{-1}$. Figure 1A,B shows the effect of direct electron exposure on a BNLC. The water in the liquid cell appears bright in the image, as it is much thicker than the carbon support or the BN covering the liquid. When the beam is positioned at the location marked in Figure 1A, despite the short duration of exposure used to avoid damaging the BNLC, the water in the path of the electron beam disappears. The dark area left by the beam that can be observed in Figure 1B is a bubble containing the gas formed by radiolysis of the water. As the gas is much less dense than the surrounding water, it appears dark in the image. To avoid this difficulty the “aloof” EELS acquisition geometry can be used. In this case, the electron beam passes typically 10–50 nm from the sample, interacting only via the evanescent field and never making direct contact.^[4,6,11] This approach avoids strong ionizing electron–sample interactions, allowing beam-sensitive samples to be examined without significant radiation damage.^[4,11] Although the signal is delocalized in the low-loss EELS region due to the nature of the phonon and plasmon excitation processes, the signal can still be analyzed at the atomic level if correlated to the corresponding atomic resolution S/TEM image of the material.^[26]

Access to the vibrational response of water requires very high energy resolution, and that in turn requires a monochromated

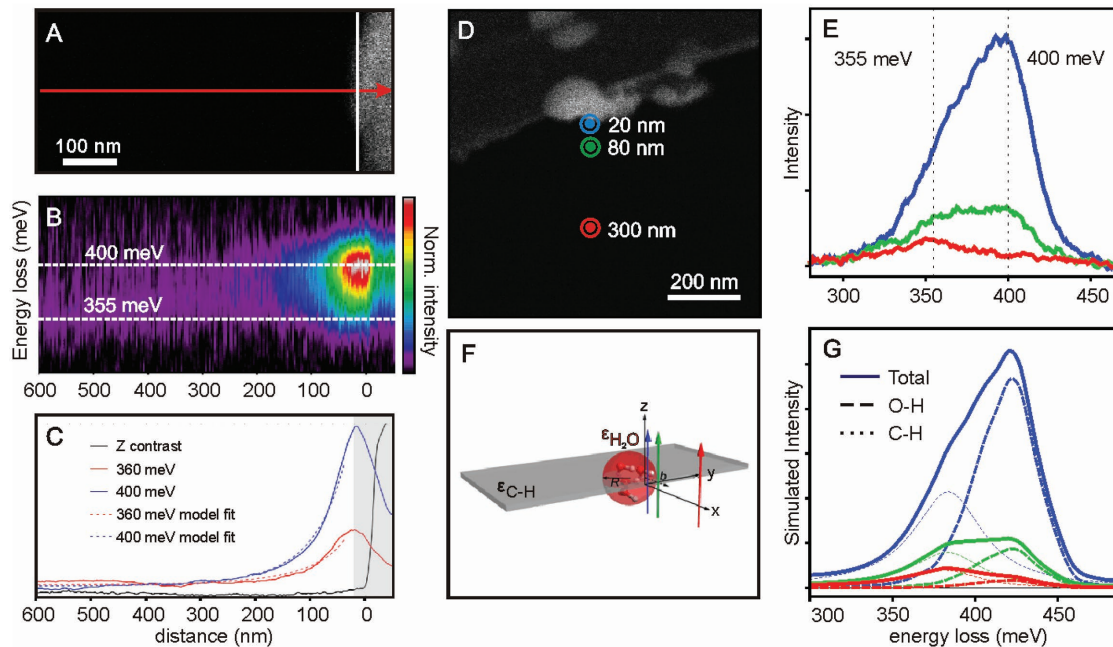


Figure 2. The effect of the impact parameter on the vibrational EELS. A) STEM image of a BNLC over the edge of a carbon support with the position of the EELS linescan shown in red. B) The dependence of the water vibrational response as a function of impact parameter. C) The experimental and modeled EELS intensity of both water (400 meV) and C–H (355 meV) signals and the intensity of the STEM-HAADF image as a function of impact parameter. D) Reference image for EEL spectra. E) Spectra taken at three impact parameters: 20 nm (blue), 80 nm (green), and 300 nm (red). F) Theoretical model for calculation of the delocalization of different vibrational modes. G) Simulated EEL spectra for the C–H (375 meV) and O–H (420 meV) stretching modes at 20 nm (blue), 80 nm (green), and 300 nm (red). Note: Simulated intensity for the EEL spectra with an impact parameter of 300 nm was multiplied by 5 for visibility.

electron beam. In EELS experiments, the spectral resolution of the instrument is commonly characterized by the full-width at half-maximum (FWHM) of the zero loss peak (ZLP). The ZLP contains all the electrons in an EELS acquisition that have undergone only elastic interactions, without energy loss. The ZLP of a standard cold-field-emission (cFEG) gun is shown in Figure 1D, with a FWHM of ≈ 285 meV. At this energy resolution, phonons peaks, with line widths of tens of meV are not detectable. Additionally, the background of the cFEG ZLP tail is still between 20 and 50% of its maximum intensity throughout the infrared (i.e., low-loss) energy regime. Since the phonon excitation through aloof electron beam interaction is inefficient, the background signal completely obscures the phonon signal in cFEG EELS. With a monochromated electron beam, however, there is over an order of magnitude improvement in spectral resolution and several orders of magnitude reduction of the EELS background without sacrificing spatial resolution.^[4] A monochromated ZLP, also in Figure 1D, shows the improved energy resolution (23 meV FWHM for this particular experiment) and the dramatically reduced background. While the ≈ 20 meV wide ZLP is still much wider than the natural phonon linewidths (≈ 1 meV/ ≈ 10 cm $^{-1}$), the improvement coupled with the reduced background allow for different vibrational modes to be directly detected with the electron probe.

To choose the optimum location of the electron beam for recording the vibrational EELS data, a STEM image was first acquired at a high scanning rate under low dose conditions to minimize the electron flux on the BNLC. The beam was then placed 10 nm from the specimen to collect the aloof spectra.

The result is shown in Figure 1E, which illustrates the monochromated, aloof-EELS response of a liquid-water-filled BNLC, strongly showing the O–H stretching vibrational mode of water at ≈ 400 meV.^[25,27]

Beyond simply measuring the vibrational response of liquids, one can reveal the spatial distribution of the vibrational signal in multicomponent systems. This is demonstrated by inspecting the effect of the distance between the electron beam and the liquid cell, known as the impact parameter. A STEM image of a water pocket on the edge of the carbon support is shown in Figure 2A, where the red arrow marks the path of an EELS linescan taken from left to right. The background subtracted spectral response along the linescan in the vibrational regime is plotted in Figure 2B, showing an apparent shift in the peak center as the beam gets closer to the BNLC. In Figure 2C, we plot the EELS intensity at 400 and 355 meV, respectively, showing a shift in the spectral weight with distance from the BNLC.

To better understand the origin of this behavior, spectra were acquired at three different impact parameters: 20 nm (blue), 80 nm (green), and 300 nm (red), shown in Figure 2D. The corresponding spectra are plotted in Figure 2E. Close to the BNLC, the response is, as expected, a strong signal from the O–H stretching mode at 400 meV. At 80 nm, the 400 meV peak is still observable and is still the strongest feature, however, the shape of the overall spectrum has changed and a second peak is clearly visible. Far away from BNLC (300 nm) the 400 meV peak completely vanished while the secondary peak at 355 meV is still present. Examining the intensity of each peak as a function

of distance from the BNLC (Figure 2C), while the intensities of the EELS peaks approach background level far away from the liquid cell, there appears to be a cross-over in spectral intensity at a distance of ≈ 300 nm. This change indicates the two peaks may arise from two independent signals.

The energy difference between the two peaks is large, and unlikely to be a result of temperature effects as those shifts are much smaller.^[28] Another possibility is the presence of a different chemical species, for example, a C–H stretching mode arising from adsorbed hydrocarbons on the holey carbon support film. The C–H signal is considered to be spatially more extended over the sample support, and thus decays slower than the O–H signal coming from the water encapsulated in the BNLC. By employing a phenomenological modeling approach,^[24,29–33] we can test this hypothesis. Figure 2F shows the dielectric model used for the theoretical calculations, where the supporting carbon is represented by an extended flat plane passivated with H atoms from adsorbed hydrocarbons. The model also includes the H₂O in the BNLC as a sphere with a 40 nm radius. The intensity of the C–H stretching mode from the adsorbed hydrocarbons and the O–H stretching mode from the liquid cell (at their theoretical values of 375 and 420 meV, respectively) are calculated at impact parameters of 20, 80, and 300 nm. The results are plotted in Figure 2G, which show agreement in line-shape and intensity with respect to the experimental results (Figure 2E).

There are a few differences between the simulated and measured spectra that warrant attention. Notice that the water contribution, calculated with the dielectric function of bulk water, exhibits the peak at 420 meV (arising from the O–H stretching modes), which is 20 meV shifted compared to the experimental spectra. Hence, to reproduce the spectral shape, the modeled C–H vibration was also set to a consistently higher energy compared to the experiment. We note that this difference may arise due to nanoconfinement of the water molecules or an interaction with h-BN encapsulating layers, which could change the energy of the O–H stretching modes. It also should be noted that for the simulated EEL spectra at an impact parameter of 300 nm, the intensity is scaled up by a factor of 5 to match the experimental intensity and for visibility in the figure. This is likely caused by our particular assumption of the amount and orientation of C–H in the surrounding area, which varies due to the irregular shape of the supporting holey carbon grid. However, the 20 and 80 nm impact parameters match both quantitatively and qualitatively, indicating that the location of both surface modes originating from the water and from adsorbed species can be distinguished. These results show that the content and distribution of beam-sensitive matter excitations can be deciphered via a combination of EELS and simulation.

Vibrational spectroscopies are also sensitive to small changes in mass, allowing identification of isotopes. Deuterium oxide (or ¹³C) is often used for isotopic labeling in studies involving biological materials or for gaining deeper insights into the physics of water.^[28,34] The heavier isotope should be visible as a peak at lower energy loss. In the present case, we use this isotope sensitivity to validate the identity of the water vibrational peak in EELS using samples containing a mixture of D₂O and H₂O. Figure 3 compares the average of 100 spectra from a sample with H₂O and from a second sample with a

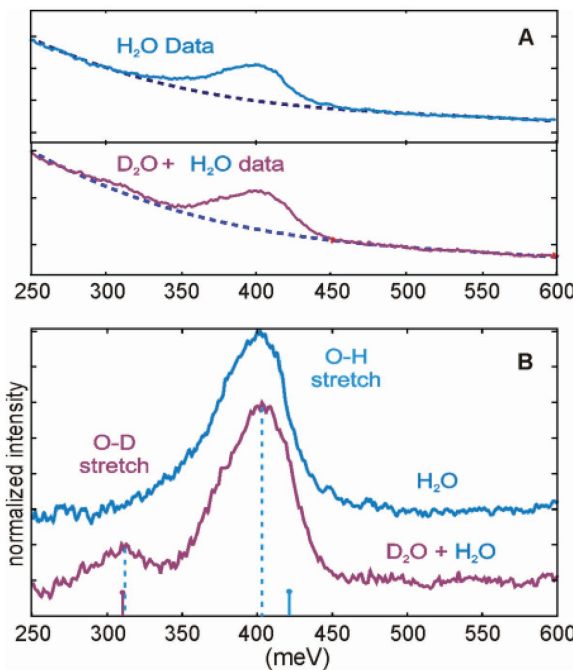


Figure 3. Comparison of H₂O and D₂O vibrational EELS. A) EEL spectra of O–H peak for H₂O and D₂O and the polynomial fit used for background subtraction (dashed lines). B) Background subtracted EEL spectra of H₂O and a D₂O/H₂O mixture showing clear signatures of the H₂O O–H peak at 400 meV and the D₂O stretching peak at 310 meV. The expected positions of the H₂O (421 meV, 3400 cm⁻¹) and D₂O (310 meV, 2500 cm⁻¹) peaks from IR data in literature are indicated by the vertical lines at the bottom.

D₂O + H₂O mixture. The spectra were acquired at a constant impact parameter of ≈ 10 nm from the liquid cell and an electron probe monochromated to 20 meV (FWHM). The as-acquired data are shown in Figure 3A, with the corresponding fit to the background and the background-subtracted spectra, is shown in Figure 3B. While the O–H stretching peak at 400 meV is observable in both, the O–D stretch at 310 meV is visible only in the H₂O–D₂O mixture. It is notable that the O–H peak at 400 meV is offset from the expected energy of ≈ 420 meV, while the O–D peak clearly matches its expected value. A wide band of N–H and N–H₂ stretching modes has been recorded in the energy range between 372 and 409 meV using monochromated EELS and in optical spectroscopy^[15,35,36] and there is a possibility that some N–H_x, with a resonance of ≈ 400 meV, has adsorbed on the BN surface during the sample preparation.^[37] However, we expect this effect to be very small due to its low concentration with respect to water. Alternatively, this offset may be a result of different interactions occurring between the BN and the light versus the heavy water. It may also be an effect related to the confinement of the liquids in the BNLC. The investigation of such nanoscale influences on vibrational modes is not included here, but will likely be the source of many future experimental and computational research studies. Regardless, the presence of the O–D peak demonstrates that, similar to Raman and Fourier transform infrared (FTIR) spectroscopy, EELS is sensitive to isotopic species, at high spatial resolution using very small samples.

We have demonstrated isotope labeling via EELS for the first time, which can be used in any system where the spatial resolution of the electron microscope combined with chemical information from vibrational spectroscopy is required. Such capabilities are possible as the BN window material has a low background signal. A well-defined spectral window where the h-BN peak can be observed^[27] limits the overlap of signals and allows for the discrimination of the isotope signatures. Furthermore, the lower damage threshold for BN over graphene liquid cells can be overcome by combining vibrational EELS with cryo-TEM and damage-free techniques, such as leapfrog scanning.^[10] Key applications may involve labeling and mapping of organic or biological materials, including isotope detection to track the progress of chemical reactions or biological processes, such as in proteomics and medicine.^[38,39]

Finally, the ability to distinguish between phonon modes based on the geometry and delocalization of the vibrational signal brings the potential to examine many problems in physics, such as surface passivation in beam-sensitive catalysts and photovoltaics/photocatalysts.^[40] Therefore, it is possible to envision utilizing isotope-labeled EELS (IL-EELS) to characterize dynamic processes by integrating the BNLC sample geometry with conventional membrane-type liquid cell holders. Such integration would alleviate some of the limitations of the current BNLC design, enabling liquid flow through the BNLC, electrical biasing, heating, or cooling. Even in the case of thicker windows or liquid layers, this approach will be feasible since the only effect of sample (or window thickness) on the EELS peaks will be a diminished peak intensity. The shapes and energies of the phonon peaks should not be affected.

In conclusion, we have shown that our new approach to vibration EELS of liquids enables us to address many exciting scientific problems. For example, changes in the structure and orientation of water (and other liquids) next to solid surfaces, solidification fronts, suspended nanoparticles, or in reactive systems utilizing flow and isotope labeling now become possible. As modern technology and science depends on understanding the detailed interactions at such nanoscopic interfaces, vibrational EELS should find broad application in many disciplines.

Experimental Section

Liquid Sample Preparation: BN liquid cells were prepared using commercial chemical vapor deposition (CVD) grown BN on copper substrates (Graphene Supermarket, Inc.). The Cu substrate was removed by etching in commercial ammonium peroxydisulfate (APS) etchant (Transene, Inc.) solution, and the free-floating BN was then transferred to pure water. The BN grid was assembled in several steps. First, a layer of BN was applied to a plasma-cleaned lacey carbon grid by touching the lacey carbon-coated side of the grid to a floating piece of BN. The grid was then thoroughly dried under an IR lamp. A very small (3 μ L) droplet of purified water was then pipetted onto the dried grid. This droplet is the water to be encapsulated. A second layer of BN was then applied to the wetted surface by capture of a second piece of BN from the liquid surface in the same manner as the first layer. After the application of the second layer, the specimen was allowed to air dry for ~20 min, then placed in a vacuum desiccator. The liquid cells were sealed by the Van der Waals interaction between the two BN layers and the surface tension of the water droplets. D₂O–H₂O samples were prepared similarly, with one additional transfer of the BN to pure D₂O prior to assembling the

liquid cells, and pipetting D₂O as the sample material before picking up the second BN layer. A schematic of the process is included in Figure S4 (Supporting Information). For all specimens prepared in this way, the majority of water pockets were, on average, ≈20–50 nm in thickness measured by analyzing the low-loss region of the EELS spectrum, separately acquired from the phonon measurement using a JEOL ARM200CF.

Nion Microscope Image Acquisition and Processing: All vibrational spectra shown in this manuscript were collected on the Nion's aberration-corrected high-energy-resolution monochromated EELS-STEM (HERMES) at Oak Ridge National Laboratory operated at 60 kV accelerating voltage. The microscope is equipped with a prototype Nion spectrometer possessing a Hamamatsu ORCA high-speed, low-noise SC莫斯 detector. All EEL spectra were acquired with a 1 mm aperture corresponding to a collection angle of 13 mrad, a probe with a convergence angle of 15 mrad, and a beam current of ≈300 pA. Additionally, all EEL spectra were produced by acquiring multiple acquisitions, and subsequently using subpixel alignment to create a single summed spectrum, with the goal of minimizing the effect of tip-noise on the EELS. To fit and subtract the backgrounds for the spectra in Figures 2 and 3, a third-order exponential ($e^{-ax^3-bx^2-cx-d}$) is fit to the background on either side of H₂O/D₂O vibrational regime, on one side between 220 and 280 meV and on the other between 475 and 550 meV. It was chosen not to use a power-law background for fitting peaks on the tails of the monochromated ZLP as the convolution of the monochromation with the standard Fowler–Nordeheim distribution of the field emission zero-loss peak is modeled more effectively by the third-order exponential. STEM images were acquired at 512 \times 512 pixel density. EEL spectra and STEM images were processed using NionSwift software (Nion, Co.) and Digital Micrograph (Gatan, Inc.). Processing of the EELS was accomplished either with NionSwift software and using in-house add-on Python scripts. Annotations were added to the figures using CorelDraw.

Simulation: Details of the simulation and the model used for calculation are included in the Supporting Information.

Supporting Information

Supporting Information is available from the Wiley Online Library or from the author.

Acknowledgements

J.R.J. and J.A.H. contributed equally to this work. Microscopy research performed as part of a user proposal at Oak Ridge National Laboratory's Center for Nanophase Materials Sciences (CNMS), which is a U.S. Department of Energy, Office of Science User Facility (J.A.H., J.C.I.). This research was conducted, in part, using instrumentation within ORNL's Materials Characterization Core provided by UT-Battelle, LLC under Contract No. DE-AC05-00OR22725 with the U.S. Department of Energy. This manuscript was authorized by UT-Battelle, LLC under Contract No. DE-AC05-00OR22725 with the U.S. Department of Energy. The U.S. Government retains and the publisher, by accepting the article for publication, acknowledges that the U.S. Government retains a nonexclusive, paid-up, irrevocable, worldwide license to publish or reproduce the published form of this manuscript, or allow others to do so, for U.S. Government purposes. The Department of Energy will provide public access to these results of federally sponsored research in accordance with the DOE Public Access Plan (<http://energy.gov/downloads/doe-public-access-plan>). Acquisition of UIC JEOL ARM200CF was supported by an MRI-R² grant from the National Science Foundation (DMR-0959470). The Gatan Quantum GIF acquisition at UIC was supported by an MRI grant from the National Science Foundation (DMR-1626065). Theoretical simulations were supported by Spanish Ministry project FIS2016-80174-P.

Conflict of Interest

O.L.K., N.D., and T.L. have a financial interest in Nion Co. which manufactured the microscope used for this study.

Keywords

EELS, liquid cells, nanoscale, spectroscopy, STEM

Received: April 27, 2018

Revised: June 2, 2018

Published online:

- [1] Y. Ni, J. L. Skinner, *J. Chem. Phys.* **2016**, *145*, 124509.
- [2] S. K. Natarajan, J. Behler, *Phys. Chem. Chem. Phys.* **2016**, *18*, 28704.
- [3] O. Byl, J. C. Liu, Y. Wang, W. L. Yim, J. K. Johnson, J. T. Yates Jr., *J. Am. Chem. Soc.* **2006**, *128*, 12090.
- [4] O. L. Krivanek, T. C. Lovejoy, N. Dellby, T. Aoki, R. W. Carpenter, P. Rez, E. Soignard, J. Zhu, P. E. Batson, M. J. Lagos, R. F. Egerton, P. A. Crozier, *Nature* **2014**, *5*, 209.
- [5] M. J. Lagos, A. Trügler, U. Hohenester, P. E. Batson, *Nature* **2016**, *543*, 529.
- [6] P. A. Crozier, *Ultramicroscopy* **2017**, *180*, 104.
- [7] P. A. Crozier, T. Aoki, Q. Liu, *Ultramicroscopy* **2016**, *169*, 30.
- [8] R. F. Egerton, *Ultramicroscopy* **2015**, *159*, 95.
- [9] G. Radtke, D. Taverna, M. Lazzari, E. Balan, *Phys. Rev. Lett.* **2017**, *119*, 027402.
- [10] R. F. Egerton, T. Aoki, P. A. Crozier, *MSA 2016 Proc.* **2016**, 960.
- [11] P. Rez, T. Aoki, K. March, D. Gur, O. L. Krivanek, N. Dellby, T. C. Lovejoy, S. G. Wolf, H. Cohen, *Nat. Commun.* **2016**, *7*, 10945.
- [12] T. Miyata, M. Fukuyama, A. Hibara, E. Okunishi, M. Mukai, T. Mizoguchi, *Microscopy* **2014**, *63*, 377.
- [13] T. Schmid, B-S. Yeo, G. Leong, J. Stadler, R. Zenobi, *J. Raman Spectrosc.* **2009**, *40*, 1392.
- [14] M. Jin, F. Lu, M. A. Belkin, *Light: Sci. Appl.* **2017**, *6*, e17096.
- [15] C. Dwyer, T. Aoki, P. Rez, S. L.Y. Chang, T.C. Lovejoy, O.L. Krivanek, *Phys. Rev. Lett.* **2016**, *117*, 256101.
- [16] N. De Jonge, F. M. Ross, *Nat. Nanotechnol.* **2011**, *6*, 695.
- [17] H. Zheng, H. Smith, R. K. Y.-W. Jun, C. Kisielowski, U. Dahmen, A. P. Alivisatos, *Science* **2009**, *324*, 1309.
- [18] F. M. Ross, *Science* **2015**, *350*, 9866.
- [19] M. E. Holtz, Y. Yu, J. Gao, H. D. Abruna, D. A. Muller, *Microsc. Microanal.* **2013**, *19*, 1027.
- [20] C. Wang, Q. Qiao, T. Shokuhfar, R. F. Klle, *Adv. Mater.* **2014**, *26*, 3410.
- [21] J. M. Yuk, J. Park, P. Ercius, K. Kim, D. J. Hellebusch, M. F. Crommie, J. Y. Lee, A. Zettl, A. P. Alivisatos, *Science* **2012**, *336*, 61.
- [22] A. J. Donovan, J. Kalkowski, M. Szymusiak, C. Wang, S. A. Smith, R. F. Klle, J. H. Morrissey, Y. Liu, *Biomacromolecules* **2016**, *17*, 2572.
- [23] H. Cho, M. R. Jones, S. C. Nguyen, M. R. Hauwiller, A. Zettl, A. P. Alivisatos, *Nano Lett.* **2017**, *17*, 414.
- [24] C. Kisielowski, L.-W. Wang, P. Specht, H. A. Calderon, B. Barton, B. Jiang, J. H. Kang, R. Cieslinski, *Phys. Rev. B* **2013**, *88*, 024305.
- [25] J. C. Idrrobo, W. Zhou, *Ultramicroscopy* **2017**, *180*, 156.
- [26] W. Zhou, J. Lee, J. Nanda, S. T. Pantelides, S. J. Pennycook, J. C. Idrrobo, *Nat. Nanotechnol.* **2012**, *7*, 161.
- [27] A. A. Goyadinov, A. Konecna, A. Chuvalin, S. Velez, I. Dolado, A. Y. Nikitin, S. Lopatin, F. Casanova, L. E. Hueso, J. Aizpurua, R. Hillenbrand, *Nat. Commun.* **2017**, *8*, 95.
- [28] S. A. Corcelli, J. L. Skinner, *J. Phys. Chem. A* **2005**, *109*, 6154.
- [29] F. J. García de Abajo, *Rev. Mod. Phys.* **2010**, *82*, 209.
- [30] G. M. Hale, M. R. Querry, *Appl. Opt.* **1973**, *12*, 555.
- [31] F. J. García de Abajo, *Phys. Rev. B* **1999**, *59*, 3095.
- [32] T. L. Ferrell, P. M. Echenique, *Phys. Rev. Lett.* **1985**, *55*, 1526.
- [33] R. Garcia-Molina, A. Gras-Marti, A. Howie, R. H. Ritchie, *J. Phys. C* **1985**, *18*, 5335.
- [34] Z. Wang, A. Pakoulev, Y. Pang, D. D. Dlott, *J. Phys. Chem. A* **2004**, *108*, 9054.
- [35] B. Singh, G. Kaur, P. Singh, K. Singh, B. Kumar, A. Vij, M. Kumar, R. Bala, R. Meena, A. Singh, A. Thakur, A. Kumar, *Sci. Rep.* **2016**, *6*, 35535.
- [36] C. Tang, Y. Bando, Y. Huang, C. Zhi, D. Golberg, *Adv. Funct. Mater.* **2008**, *18*, 22.
- [37] D. M. Haiber, P. A. Crozier, *ACS Nano* **2018**, *12*, 5463.
- [38] H. Jiang, E. Favaro, C. N. Goulbourne, P. D. Rakowska, G. M. Hughes, M. G. Ryadnov, L. G. Fong, S. G. Young, D. J. P. Ferguson, A. L. Harris, C. R. M. Grovenor, *Methods* **2014**, *68*, 317.
- [39] C. Lechene, F. Hillion, G. McMahon, D. Benson, A. M. Kleinfield, J. P. Kampf, D. Distel, Y. Luyten, J. Bonventre, D. Hentschel, K. M. Park, S. Ito, M. Schwartz, G. Benichou, G. Slodzian, *J. Biol.* **2006**, *5*, 20.
- [40] J. A. Hachtel, A. R. Lupini, J. C. Idrrobo, *Sci. Rep.* **2018**, *8*, 5637.